Giant, 18, 2024, 100267

Compatibilized polylactide/poly(pentamethylene furanoate) blends for fully bioderived packaging films with enhanced fracture toughness and UV- and O_2-barrier properties

Full-length article

Giulia Fredi [a,*], Davide Perin [a], Carlotta Zardo [a], Marco Rapisarda [b], Paola Rizzarelli [b], Michelina Soccio [c,d,e], Nadia Lotti [c,d,f], Andrea Dorigato [a]

[a] Department of Industrial Engineering and INSTM Research Unit, University of Trento, Via Sommarive 9, 38123, Trento, Italy
[b] Institute for Polymers, Composites and Biomaterials (IPCB) – Catania, Via P. Gaifami 18, 95126, Catania, Italy
[c] Department of Civil, Chemical, Environmental and Materials Engineering, University of Bologna, Via Terracini 28, Bologna, 40131, Italy
[d] Interdepartmental Center for Industrial Research on Advanced Applications in Mechanical Engineering and Materials Technology, CIRI-MAM, Viale del Risorgimento 2, 40136, Bologna, Italy
[e] Interdepartmental Center for Industrial Research on Buildings and Construction CIRI-EC, Via del Lazzaretto 15/5, 40131, Bologna, Italy
[f] Interdepartmental Center for Industrial Agro-Food Research, CIRI-AGRO, Via Quinto Bucci 336, 47521, Cesena, Italy

Keywords: Polylactic acid, Furanoates, Biopolymers, Blends, Biodegradable polymers, Degradability

Polylactide (PLA) is a promising biopolymer from renewable resources but its brittleness and poor gas barrier properties limit flexible packaging applications. Therefore, in this work PLA was blended with a biobased rubbery poly(pentamethylene furanoate) (PPeF), acting as a toughening agent, and a commercial epoxy-functionalized compatibilizer (i.e., Joncryl® ADR-4468) was added to improve the interfacial interaction. The effect of PPeF loading (1–30 wt %) on phase morphology, mechanical properties, oxygen permeability, and degradability in compost was characterized. All blends displayed a sea-island morphology with refined PPeF domains upon compatibilization. Incorporating PPeF induced major tensile ductility enhancements from 5 % strain at break for neat PLA up to 200 % for the blend with 30 wt % PPeF, accompanied by progressive stiffness and strength declines. Through the application of the essential work of fracture (EWF) approach on the prepared films, the specific essential work of fracture (w_e) was seen climbing from 6.2 to 40.0 kJ/m^2 with rising PPeF content, confirming its effectiveness

* Corresponding author.
E-mail address: giulia.fredi@unitn.it (G. Fredi).
Received 8 January 2024; Received in revised form 26 March 2024; Accepted 9 April 2024

 https://doi.org/10.1016/j.giant.2024.100267

as a toughness enhancer. PPeF contributed to increase the UV- and gas barrier properties of PLA. For example, the oxygen permeability dropped by 37 % for the blend with 30 wt % PPeF. Moreover, compost burial tests also revealed 26 % weight loss of PPeF after 60 days, proving its biodegradability. Hence, finely dispersed PPeF domains induced synergistic property improvements, making PLA/PPeF blends a promising sustainable option for flexible and biodegradable packaging.

1 Introduction

Plastics have become an indispensable material in the modern society, offering unmatched versatility, processability, and cost-effectiveness. They enable technological innovations in all fields and are especially prevalent in packaging applications, representing about 40 % of the total plastics demand [1]. Packaging constitutes a key element in the modern food supply chain, ensuring protection and extending the shelf life of perishable goods. At the same time, the large and rapidly growing consumption of plastic packaging raises severe environmental concerns, as most of it is produced from non-renewable petrochemical resources and does not biodegrade at the end of its life. The plastic waste accumulating in landfills and in the natural environment is increasingly perceived as unacceptable by public opinion [2].

In this context, bioplastics, defined as plastics that are bio-based, biodegradable, or both [3], are attracting growing interest. Bioderived bioplastics allow for the reduction of the carbon footprint in the production phase by using renewable biological resources instead of fossil fuels. Additionally, biodegradable bioplastics offer alternative waste disposal routes compared to the persistent accumulation of conventional plastics [4]. However, nowadays bioplastics still account for less than 1 % of total plastics production worldwide [5]. The main barriers to their widespread adoption are high production costs and inferior performance compared to traditional petroleum-based plastics. Intensive research and development efforts are ongoing to improve the properties of bioplastics, enhance their processability, and reduce their price, to make them economically and environmentally competitive with conventional plastics [6,7].

Among the most promising bioplastics for packaging is polylactic acid (PLA), a biopolymer derived from renewable resources such as corn starch or sugarcane. PLA exhibits good stiffness and strength combined with transparency, printability, and compostability under industrial conditions [8–11]. This makes it an excellent candidate to replace commodity plastics like poly(ethylene terephtalate) (PET) in rigid packaging applications. However, the brittleness and low impact resistance of PLA limit its use in flexible packaging and require the addition of plasticizers or blending with a ductile polymer phase [12]. Much research has been dedicated to toughening PLA while preserving its stiffness, via the addition of low molecular weight plasticizers or via blending with tough polymers, with moderate success so far [13]. An interesting class of candidate polymers for PLA toughening are the furanoate polyesters, derived from 2,5-furandicarboxylic acid (FDCA). FDCA is produced by the catalytic dehydration of carbohydrate feedstocks like glucose and represents a promising renewable alternative to terephthalic acid for polyester synthesis [14–16]. Poly(alkylene furanoate)s (PAFs) exhibit excellent gas barrier properties, making them promising materials for food packaging, and possess a wide range of tunable properties depending on the length of the alkylene glycol segment [17,18]. Hence, blending PAFs with PLA could synergistically combine the high stiffness of PLA with the ductility of PAFs, thus producing a biopolymer film with balanced mechanical properties and improved gas barrier performance [19–21].

Among the PAF family, poly(pentamethylene furanoate) (PPeF) displays an unusual combination of properties, being amorphous and rubber-like at room temperature and still exhibiting remarkable UV-shielding capability and excellent gas-barrier properties, comparable to ethylene-vinyl alcohol copolymers [22,23]. This suggests it could effectively enhance the gas barrier properties of PLA while also improving its ductility and fracture toughness. This has been recently proven by our group, which developed PLA/PPeF films with remarkable strain at break and interesting gas barrier properties, and proved their selective recyclability via enzymatic recycling [24,25]. Although showing promising results, those films were produced via solution casting, a non-scalable and environmentally unfriendly technique. Moreover, PLA and PPeF resulted as immiscibile, with a typical coarse sea-island morphology. Hence, the addition of a suitable compatibilizer revealed itself as essential to stabilize the morphology and enable effective stress transfer across the PLA/PPeF interface. Reactive processing with epoxy-functionalized chain extenders represents an effective compatibilization strategy for PLA-based systems, promoting in-situ grafting reactions.

For PLA/PAF blends produced by solution mixing, our research group previously showed improved ductility and fracture toughness with PAFs like PBF, PPeF, and other longer alkyl chain PAFS, although phase adhesion was poor [24,26-32]. We also recently demonstrated significant property improvements for blends with PLA and PEF, PPF, and PBF produced from the melt and compatibilized with an epoxy-functionalized styrene-acrylic oligomer (Joncryl® ADR-4468) [33,34]. However, no studies have explored the compatibilization of PLA/PPeF blends processed in the melt, which enables industrially relevant manufacturing methods like extrusion and injection molding. Moreover, no studies have ever investigated the biodegradability or composting ability of such blends, although previous studies have demonstrated the degradability in compost of some FDCA-based copolyesters [35,36].

Hence, the present work aims to develop PLA/PPeF blend films with finely dispersed PPeF domains, strong interfacial adhesion, and enhanced fracture toughness, by reactive compatibilization with Joncryl® ADR-4468 as a multifunctional compatibilizer/chain extender. The blends were characterized regarding thermal properties, phase morphology, oxygen permeability, degradability under compost burial conditions, optical transparency, and mechanical performance. Moreover,

the fratcure behavour of the prepared films was assessed through the essential work of fracture (EWF) approach [37]. More broadly, this work provides new insights into the development of high-performance bioplastic blends from renewable resources. Understanding blend morphology and properties guides efforts to replace conventional plastics with high-performing and functionally tailored bioplastic materials.

2 Materials and methods

2.1 Materials

The PLA used in this work was the extrusion-grade Ingeo™ Biopolymer 2500HP, provided by NatureWorks LLC (Minnetonka, MN, USA). This polymer was provided in the form of pellets and showed a density of 1.24 g/cm^3 and a melt flow index of 8 g/10 min (210 °C; 5 kg). PPeF was synthesized via a two-stage polycondensation synthesis, as described in a previous work of our group [22]. The resulting PPeF had a number-average molecular weight (M_n) of 29,600 g/mol. The employed compatibilizer/chain extender was a poly(styrene-acrylic-co-glycidyl methacrylate) (SAGMA), commercially known as Joncryl® ADR 4468 (J), supplied by BASF Gmbh (Ludwigshafen am Rhein, Germany). This multifunctional reactive component was provided in the form of transparent flakes with an average dimension of 2.5–4.0 mm, a density of 1.08 g/cm^3, a glass transition temperature (T_g) of 59 °C, an M_n of 7250 g/mol, and an epoxy equivalent weight of 310 g/mol. All commercial materials were used as received.

2.2 Sample preparation

PLA/PPeF blends compatibilized by J were produced through melt compounding in a Haake™ Rheomix PolyLab™ System (Thermo Scientific, Waltham, MA, USA), equipped with two counter-rotating rotors. Before use, PLA granules were dried under vacuum at 80 °C for three days, while PPeF was kept at 30 °C under vacuum for seven days. The rotational speed of the rotors was set to 60 rpm, and PLA and PPeF were slowly poured into the working chamber, operating at 190 °C After 2 min, J was added. The total time interval between the start of mixing and the extraction of the compound was set to 10 min. During the procedure, it was observed that the addition of J led to an increase in the torque until it reached a plateau, as expected, due to the increase in molecular weight and chain branching caused by the compatibilizer. The obtained blends were further processed by hot pressing to produce square plates 120 mm wide and 2 mm thick using a Carver hot press, at 190 °C for 5 min, with an applied pressure of 3.4 MPa.

Additionally, small pieces cut out from these plates have been further hot-pressed to prepare thin films. Approx. 9 g of each plate were hot-pressed at 1 MPa for 5 min at 190 °C without a confining mold, to obtain films with nominal dimensions of 30 × 30 cm^2 and a thickness ranging between 80 and 220 μm.The obtained thickness variability is related to the large variability in viscosity across the different compositions, which caused the material to spread differently under the same applied pressure. For the purpose of the presented characterization, such variability in thickness can be accepted and does not affect the general conclusions of the work. The same hot pressing procedure was applied to neat PPeF, for which a smaller film was obtained, due to the scarcity of the material available.

Table 1

List of the prepared blends with their nominal composition.

Sample name	PLA (wt %)	PPeF (wt %)	J (phr)
PLA	100	0	0
PLA-J1	100	0	1
PLA-PPeF1-J1	99	1	1
PLA-PPeF3-J1	97	3	1
PLA-PPeF5-J1	95	5	1
PLA-PPeF10	90	10	0
PLA-PPeF10-J1	90	10	1
PLA-PPeF20-J1	80	20	1
PLA-PPeF30-J1	70	30	1

Samples were prepared with a PPeF concentration variable from 1 wt % to 30 wt % and with a fixed J concentration of 1 phr, which has been recognized as the most effective in previous works on similar PLA/PAF blends [33,34]. Samples of neat PLA, PLA containing 1 phr of J, and uncompatibilized PLA containing 10 wt % of PPeF were also prepared for comparison. The list of all the prepared compositions is shown in Table 1.

2.3 Characterization techniques

2.3.1 Rheological properties

The rheological properties of the produced blends were measured using a Discovery HR-2 hybrid rheometer (TA instrument, New Castle, DE, USA) in a parallel-plate arrangement (gap = 1.9 mm) and a frequency sweep mode ranging from 0.05 to 600 rad/s at 190 °C. The tests were carried out on laser-cut disk specimens with a nominal diameter of 25 mm and a thickness of 2 mm. These tests allowed for the determination of the complex viscosity (η^*), the shear storage and loss moduli (G', G''), and the loss factor ($tan\delta$) as a function of frequency. One specimen was tested for each composition.

2.3.2 Structural and morphological properties

The microstructural properties of the prepared blends were analyzed via a field-emission scanning electron microscope (FE-SEM) Zeiss Supra 40 (Carl Zeiss AG, Oberkochen, Germany), by analyzing the tensile fracture surface and the cryofracture surface of the prepared blends after Pt-Pd sputtering.

Fourier-transform infrared (FT-IR) spectroscopy was performed in attenuated total reflectance (ATR) mode on the surface of the prepared samples via a Perkin-Elmer Spectrum One IR spectrometer (Perkin Elmer GmbH, Waltham, MA, USA), equipped with a ZnSe crystal. 20 scans were superimposed for each spectrum in a wavenumber range 650–4000 cm^{-1} (resolution = 4 cm^{-1}). One specimen was tested for each formulation.

2.3.3 Thermal properties

Thermogravimetric analysis (TGA) was carried out with a Mettler TG50 thermobalance (Mettler Toledo, Columbus, OH, USA). Specimens of approx. 20 mg were cut from the prepared plates and subjected to a heating ramp of 10 °C/min from room

temperature up to 700 °C, under a nitrogen flow of 20 ml/min. The tests allowed measuring the temperatures associated with a mass loss of 1 wt %, 3 wt %, and 5 wt % ($T_{1\%}$, $T_{3\%}$, $T_{5\%}$), the onset degradation temperature (T_{onset}) via the tangent method, the degradation temperature (T_d), corresponding to the peak of the derivative thermogravimetry (DTG) curve, and the final mass after the test (m_r). One specimen was tested per composition.

Differential scanning calorimetry (DSC) was carried out with a Mettler DSC30 calorimeter (Mettler Toledo, Columbus, OH, USA) on specimens of approx. 10–20 mg cut from the prepared plates. The specimens were subjected to a heating-cooling-heating cycle at 10 °C/min between −50 °C and 250 °C, under a nitrogen flow of 100 ml/min. One specimen was measured per each composition. The test resulted in the determination of the glass transition temperature (T_g) of the PLA and PPeF phases and the melting, crystallization, and cold crystallization temperatures and enthalpies (T_m, T_c, T_{cc}, ΔH_m, ΔH_c, ΔH_{cc}) of the PLA phase. The degree of crystallinity of PLA (χ_{PLA}) was calculated via Eq. (1) [38]:

$$\chi = \frac{\Delta H_m - \Delta H_{cc}}{\Delta H_0 \cdot \omega} \cdot 100 \quad (1)$$

where ΔH_0 is the theoretical melting enthalpy of PLA, equal to 93.7 J/g, [39], and ω is the weight fraction of PLA.

Dynamic-mechanical thermal analysis (DMTA) was carried out in a DMA 800 (TA Instruments, New Castle, DE, USA) in single cantilever bending mode. The specimens had nominal dimensions of 35 × 10 × 3 mm^3 and the distance between the grips was fixed at 17.5 mm. Storage and loss moduli (E' and E'') and loss factor ($tan\delta$) were measured between −20 °C and 150 °C, at a heating rate of 3 °C/min, with a strain amplitude of 0.05 % and a frequency of 1 Hz. One specimen was tested for each composition.

2.3.4 Mechanical properties

Tensile tests were conducted with an Instron® 5969 electromechanical testing machine (Norwood, MA, USA), equipped with a 1-kN cell, on dumbbell 1BA specimens (ISO 527–2) laser-cut from the compression molded plates. First, at least five specimens for each sample were tested at 0.25 mm/min until a strain value of 0.3 % for the determination of the Young's modulus (E), and an extensometer (gage length = 12.5 mm) was used to measure the strain. Young's modulus was determined in the initial linear portion of the stress-strain curve as the slope between the points at strain values of 0.05 % and 0.25 %. Then, at least five additional specimens were tested at 10 mm/min until rupture, to determine the stress and strain at yield (σ_y, ε_y) and at break (σ_b, ε_b).

Because some of the examined materials exhibited ductile fracture behavior, the fracture resistance of the prepared films was investigated through an elastoplastic fracture mechanics approach, based on the essential work of fracture (EWF) under plane-strain conditions. This method has lately received a lot of interest for characterizing ductile polymeric films for packaging applications because it has the advantage of making a clear distinction between essential (surface-related) and non-essential (volume-related) work of fracture [37,40-42]. The EWF method assumes that the total work of fracture of notched specimens is the sum of two contributions, the first given by the work in the fracture process zone, considered essential for the generation of new fracture surfaces, and the second associated with the dissipative work outside the fracture process zone [40]. The essential work of fracture is a toughness-related material property, whereas the non-essential (or plastic) work of fracture is a geometry-dependent quantity.

EWF tests were performed on double-edged notched tension (DENT) specimens. In these tests, the specimens are subjected to a tensile load applied at a constant speed, and the output is a load-displacement curve with a maximum (F_{max}) reached at the value of displacement corresponding to crack initiation (u_{in}), after which the load decreases to zero, reached at the value of displacement u_{max}. The total work of fracture (W_f), calculated from the area under the load-displacement curve, is given by the sum of the essential work of fracture (W_e), necessary to create new surfaces, and the non-essential work of the plastic deformation zone, (W_p), as described in Eq. (2) [40,43]:

$$W_f = W_e + W_p \quad (2)$$

Both terms of Eq. (2) can be normalized by the specimen's cross-section, as described in Eqs. (3) and (4) [40,43]:

$$w_f LB = w_e LB + \beta w_p L^2 B \quad (3)$$

$$w_f = w_e + \beta w_p L \quad (4)$$

where w_f, w_e and w_p are the specific total, essential, and non-essential work of fracture, respectively, L is the ligament length, B is the specimen thickness, and β is a shape factor related to the geometry of the outer plastic dissipation zone. According to Eq. (4), values of w_f measured on specimens with different ligament lengths can be plotted as a function of the ligament length. Therefore, the intercept of the linear regression for $L = 0$ corresponds to w_e, the specific essential work of fracture, and the slope to βw_p. While w_e can be obtained directly from experimental data, w_p is known once known β, which is given for some specific geometries of the plastic deformation zone [40,43]. A more detailed description of the EWF method can be found elsewhere [44].

In this work, DENT specimens were cut out of the prepared films with a width (W) of 30 mm, a height (H) of 50 mm, and nominal ligament lengths of 5, 7, 9, 11, 13, or 15 mm. Five specimens were prepared per each ligament length per each composition. After measuring the effective ligament length on each specimen through an optical microscope, specimens were mounted on an Instron 5969 testing machine (grips distance = 30 mm) and tested at 10 mm/min. Data of w_f were subjected to the statistical treatment described in a recent work of our group about the application of the EWF approach on thermoplastic starch films [45]. The test allowed the determination of the specific essential work of fracture w_e, the term βw_p, and the two components of w_e related to the essential work of fracture initiation ($w_{e,in}$) and propagation ($w_{e,prop}$). These two terms were calculated from the areas under the load-displacement curves between 0 and u_{in} and between u_{in} and u_{max}, respectively, i.e., $W_{f,in}$ and $W_{f,prop}$.

2.3.5 Functional properties

The optical properties of the prepared films were investigated by a Jasco V570 UV–Vis-Near IR double beam absorption spectrometer (Easton, MD, USA). This instrument allowed measuring the transmittance (T %) of the specimens as a function of the wavelength of the incident radiation, which was generated by a tungsten filament lamp for visible and near-infrared and deuterium arc for ultraviolet. The transmittance data were collected in the range of 200–1000 nm at a scanning rate of 200 nm/min, to detect the optical behavior of the blends in the UV and visible regions.

Oxygen permeability was tested on the prepared films using the Gas Transmission Tester GTT (Brugger Feinmechanik GmbH, Munchen, Germany) at 23 °C. Each film was dried at 50 °C in vacuum for at least 24 h and then placed between the two instrument chambers, which were both evacuated for two hours. At the end of the evacuation time, the top chamber was filled with dry oxygen (1 bar) and the gas flow was set at 50 cm^3/min, while in the lower chamber a pressure sensor measured the increase in pressure as a function of time. When stationary conditions were reached, it was possible to determine the oxygen transmission rate (OTR). The tested specimens had a diameter of 10 cm, a testing area of 78.5 cm^2, and the specimen of each film. One specimen was measured for each sample.

2.3.6 Evaluation of the degradability in compost

Compost burial test was carried out at 58.0 ± 0.1 °C, under moisture-controlled conditions. Compost was provided by Biofactory S.p.A (Calcinate, BG, Italy). Triplicate specimens of film samples were placed in darkened vessels containing a multi-layer substrate [46]. Filter paper was used as a positive control. Specimens with dimensions 2 cm × 2 cm were cut out of the prepared films (initial weight 50–120 mg, filter paper ~28 mg; PA114C Ohaus Pioneer Plus, $d = 0.1$ mg) and sandwiched between two layers of a mixture of milled perlite (70 g) and compost (200 g), moistened with 100 mL of distilled water. The bottom and top layers were filled with 60 g of perlite moistened with 120 mL of distilled water. Perlite was used for increasing the aeration of the compost and the amount of water retained. Samples were removed after regular intervals (10 and 30 days), brushed softly, washed with distilled water several times and dried under vacuum in the presence of P_2O_5 at room temperature, to constant weight [47]. The degree of degradation was evaluated by weight loss (WL) by using Eq. (5):

$$WL(\%) = (W_i - W_t)/W_i \times 100 \quad (5)$$

where W_i is the initial weight of the sample and W_t is the weight after the established time.

The surface wettability was measured at room temperature using a contact angle goniometer (OCA15EC, Dataphysics). Static contact angle (SCA) values were determined by dropping 2 μL of water from a micro syringe onto the surfaces and analyzing the images taken by the connected video camera by software (SCA 20). To eliminate interference, the samples were previously equilibrated for 30 min at 40 °C and then SCA was measured. At least five measurements were carried out for each sample to ensure the repeatability of the experiments.

3 Results and discussion

3.1 Rheological properties

The rheological characterization, whose results are reported in Fig. 1(a–d), provides valuable insights into the effect of Joncryl and PPeF on the viscoelastic performance of the prepared blends in the melted state. As observed in previous works on the characterization of PLA/PAF blends [33,34], the addition of Joncryl clearly acts as a chain extender that increases the complex viscosity, storage and loss moduli, and melt elasticity of PLA. This is evidenced by the higher values of, across all frequencies for PLA-J1 over neat PLA, coupled with the disappearance of the Newtonian plateau. The increased frequency dependence and shear thinning behavior confirm the chain branching and extension induced by the compatibilizer. The incorporation of 10 wt % PPeF into PLA leads to a slight decrease in viscosity compared to neat PLA but an increase in G', particularly at low frequencies. This could depend on the lower viscosity of PPeF compared to PLA, but the increase in G', with the characteristic yield stress at low frequencies, may denote a certain surface interaction between the two polymers.

When J is added (PLA-PPeF10-J1), all rheological parameters are comparable or marginally lower than PLA-J1 alone. Complex viscosity curves corroborate the substantial viscosity enhancement observed with Joncryl addition, increasing by over an order of magnitude, and shear-thinning behavior is observed for all samples as expected. An interesting finding regarding PPeF content was that 10 wt % loading lowered viscosity compared to neat PLA, but further increasing to 30 wt % raised it again. This non-linear relation between viscosity and PPeF loading reflects the complexity of the composite systems and the interaction between components.

This manifests as more solid-like behavior, with G' exceeding G'' ($tan\delta < 1$) at a crossover frequency indicating the transition from liquid- to solid-like behavior. Without compatibilizer, PLA and PLA-PPeF10 exhibit liquid-like behavior over the whole frequency range tested. In contrast, with compatibilizer, blends show crossover frequencies from around 20 rad/s for lower PPeF contents up to 100 rad/s at higher loading, corresponding to relaxation times of 0.05–0.01 s respectively. The compatibilized blends therefore demonstrate greater elasticity, molecular cohesion, and stability against deformation from the increased chain interactions.

3.2 Structural and morphological properties

Fig. 2(a–i) shows the SEM micrographs of the cryofracture surface of the prepared blends. All samples show a typical sea-island morphology, denoting immiscibility. As found in our previous works on PLA/PAF blends [33,34], the dimension of the PPeF phase increases with the PPeF weight fraction (see also Table 2) and decreases with the introduction of J. The introduction of the compatibilizer also improves the interfacial adhesion between PLA and PPeF, but to a lesser extent compared to shorter-alkyl-chain PAFs (i.e., poly(ethylene furanoate (PEF), poly(propylene furanoate) (PPF), and poly(butylene furanoate) (PBF)) studied in previous works [33,34]. In any case, the expected microstructural refinement is evident from these micrographs, which suggests effective compatibilization.

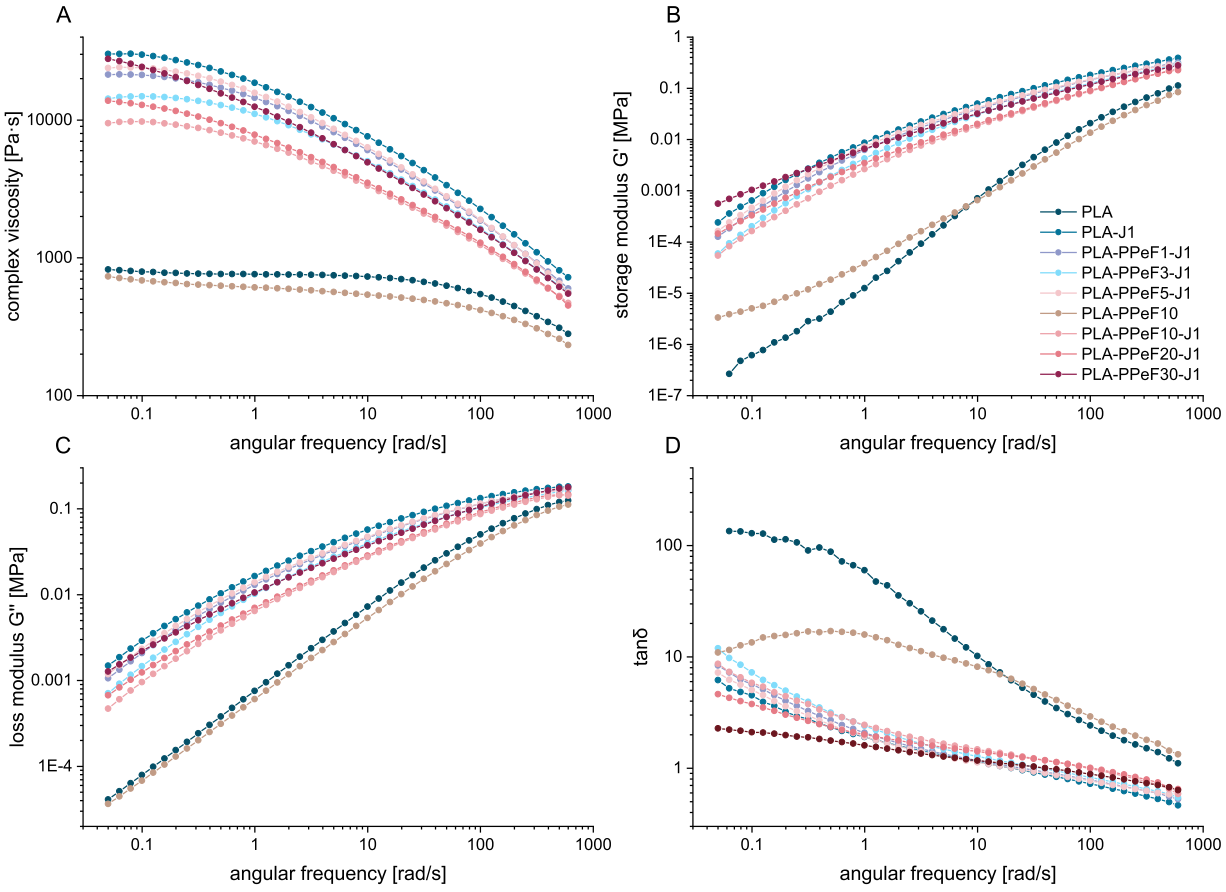

Fig. 1

Dynamic rheological test of the prepared samples. Trends of (a) complex viscosity; (b) storage modulus; (c) loss modulus; (d) tan δ as a function of the angular frequency.

Table 2

PPeF domain size for the prepared blends (mean value ± standard deviation).

Sample	PPeF domain size (μm)
PLA-PPeF1-J1	0.41 ± 0.09
PLA-PPeF10-J1	0.71 ± 0.13
PLA-PPeF20-J1	1.32 ± 0.46
PLA-PPeF30-J1	1.98 ± 0.85

The results of the ATR-FTIR characterization are reported in Fig. 3, which shows some representative compositions. PLA can be distinguished by the presence of signals associated to the -CH_3 groups. The peaks found at 1454 cm^{-1} and 1383 cm^{-1} correspond respectively to the out-of-phase bending (δ_{as}) and in-phase bending (δ_s), while the weak signals at 2997 cm^{-1} and 2946 cm^{-1} are related to the asymmetric (ν_{as}) and symmetric (ν_s) stretching. The most intense peaks are at 1752 cm^{-1} and 1181 cm^{-1}, respectively associated to the C = O ($\nu_{C=O}$) and the C–O (ν_{C-O}) groups stretching [48]. Lastly, the presence of crystalline and amorphous phases of PLA is identified by two signals at 869 cm^{-1} and 756 cm^{-1}, respectively [49].

On the contrary, PPeF can be recognized by the presence of a sharp peak at 1016 cm^{-1}, which is associated to the breathing of the furan ring [50], while the signals at 967 cm^{-1}, 823 cm^{-1} and 761 cm^{-1} are related to its bending. Moreover, the stretching of the C = C double bond ($\nu_{C=C}$), present in the furan ring, is related to the peak at 1579 cm^{-1}. The stretching of the C–O group is associated to two peaks at 1268 cm^{-1} and 1221 cm^{-1} while the stretching of the C = O group results in an intense signal at 1713 cm^{-1}. Due to the increased number of C–H bonds present in PPeF with respect to PLA, the signals associated to the methylene groups are intensified: the peaks at 2954 cm^{-1} and 2860 cm^{-1} correspond respectively to the asymmetric (ν_{as}) and symmetric (ν_s) stretching, while the signals at 1469 cm^{-1} and 1300 cm^{-1} are related to the in-phase rocking and twisting [51].

By blending PLA and PPeF, the spectra obtained are a combination of their characteristic signals, and the intensity increases or decreases according to their relative concentration. For example, the intensity of the peaks associated to PPeF (for example at 1016 cm^{-1}) progressively increases by passing from PLA-PPeF10-J1 to PLA-PPeF30-J1, while those associated to PLA (for example 1181 cm^{-1}) weaken. On the other hand, no new peaks are observed and no major red- or blue-shifts can be appreciated, which helps exclude the formation of new chemical

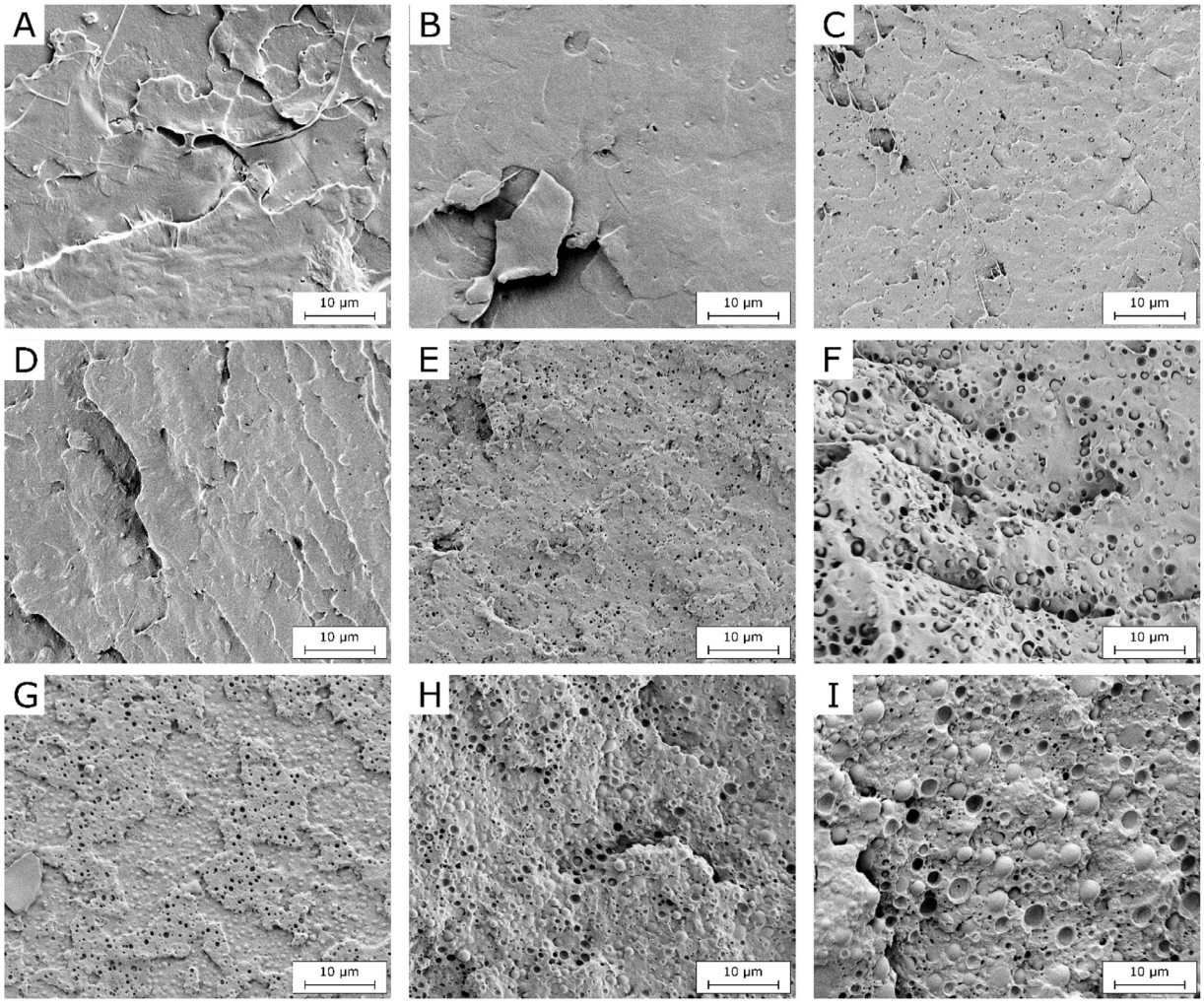

Fig. 2

SEM micrographs of the cryofracture surface of the prepared blends. (a) PLA; (b) PLA-J1; (c) PLA-PPeF1-J1; (d) PLA-PPeF3-J1; (e) PLA-PPeF5-J1; (f) PLA-PPeF10; (g) PLA-PPeF10-J1; (h) PLA-PPeF20-J1; (i) PLA-PPeF30-J1.

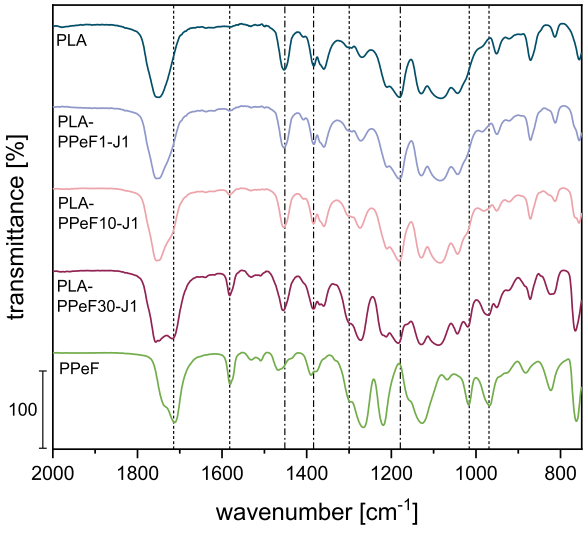

Fig. 3

ATR-FTIR spectra of some selected compositions, with the indication of the peaks related to PLA (dash-dot lines), and PPeF (dashed lines).

bonds between the two species. Some minor shifts can indeed be observed, e.g., the signal of C = O shifts from 1712 cm^{-1} in neat PPeF to 1718 cm^{-1} in PLA-PPeF30-J1 (C = O of PLA does not shift), the signal at 1266 cm^{-1} of neat PPeF shifts to 1273 cm^{-1} in PLA-PPeF30-J1, the signals located at 1081 cm^{-1} and 1181 cm^{-1} of neat PLA shift to 1088 cm^{-1} and 1183 cm^{-1} in PLA-PPeF30-J1, respectively. This may be a sign of molecular reorganization and changes in the H-binding organization after blending. However, more tests are needed to clarify this possibility, as the sensitivity of the employed ATR-FTIR instrument may be insufficient to detect small changes.

3.3 Thermal properties

The main results of the thermal characterization performed on the prepared blends are shown in Fig. 4(a –b) and in Table 3. From DSC scans (Fig. 4a), neat PLA presents a T_g of 56–58 °C and neat PPeF of 11–15 °C, in good agreement with literature data for both polymers [52,53]. PLA is also characterized by cold crystallization events at 93.7 °C and 163.7 °C and melting at 180.4 °C. On the other hand, PPeF does not undergo cold

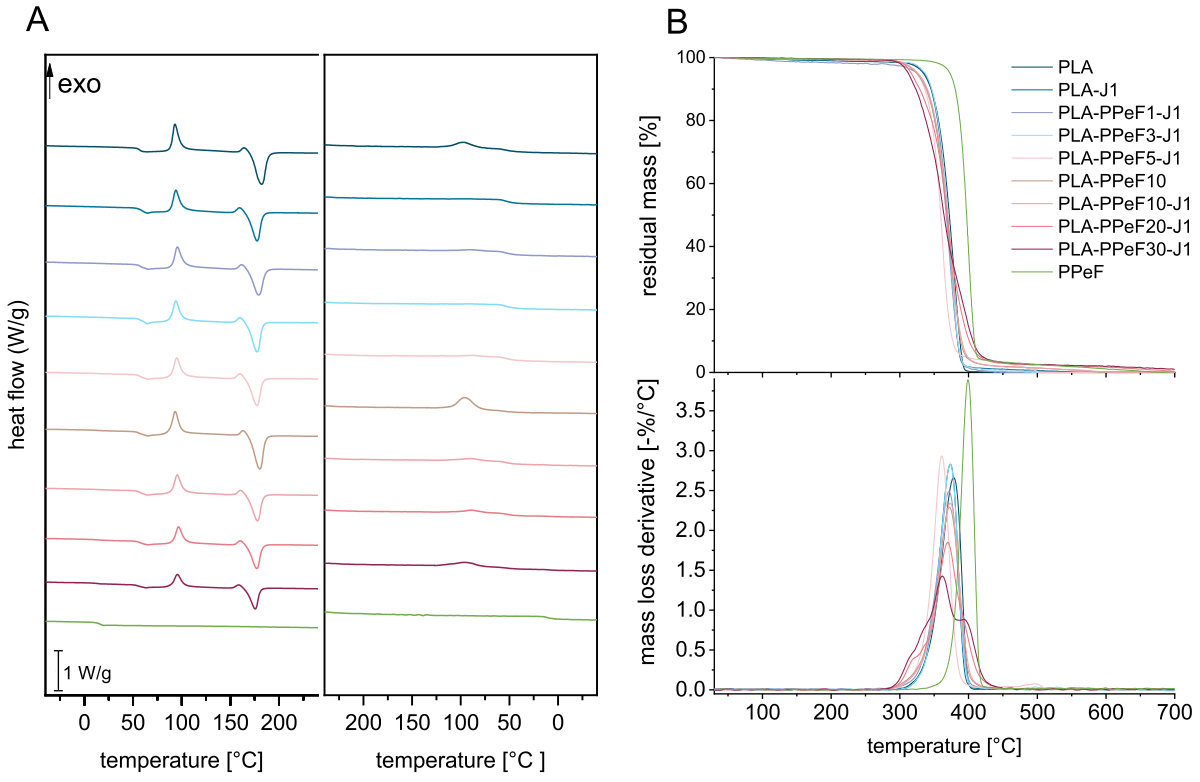

Fig. 4

Main results of the thermal analysis on the prepared blends. (a) DSC thermograms of the first heating and cooling scans; (b) TGA and DTG thermograms.

Table 3

Results of the DSC and TGA tests on the prepared blends. n.d. = not detectable; n.a. = not applicable.

	DSC										TGA	
Sample	T_g^{PPeF} (°C)	T_g^{PLA} (°C)	T_{cc1}^{PLA} (°C)	T_{cc2}^{PLA} (°C)	ΔH_{cc}^{PLA} (J/g)	T_m^{PLA} (°C)	ΔH_m^{PLA} (%)	χ_c^{PLA} (%)	T_c^{PLA} (°C)	ΔH_c^{PLA} (J/g)	T_{onset} (°C)	T_d (°C)
PLA	n.a.	56.2	93.7	163.7	34.1	180.4	54.2	21.4	98.0	17.0	327.2	378.8
PLA-J1	n.a.	58.7	94.4	159.1	31.1	175.8	42.4	12.1	92.3	0.4	329.6	373.7
PLA-PPeF1-J1	n.d.	56.6	96.1	161.3	30.7	177.8	42.4	12.9	91.0	3.5	331.2	372.2
PLA-PPeF3-J1	n.d.	61.3	94.3	159.7	29.3	176.1	43.9	16.3	90.9	1.0	334.0	373.5
PLA-PPeF5-J1	n.d.	55.9	95.2	159.5	29.7	176.1	40.7	12.5	89.2	2.2	325.9	361.0
PLA-PPeF10	n.d.	55.3	93.7	163.0	31.5	179.0	51.2	23.3	96.8	30.4	328.3	372.0
PLA-PPeF10-J1	n.d.	56.5	95.8	160.0	27.5	176.6	38.5	13.1	90.6	6.1	334.5	373.3
PLA-PPeF20-J1	14.4	56.3	96.9	159.8	25.1	175.8	34.6	12.9	89.6	5.9	307.1	370.3
PLA-PPeF30-J1	13.7	54.4	95.6	158.5	21.3	174.8	28.5	11.1	95.9	12.4	300.2	361.5
PPeF	15.7	n.a.	n.a.	n.a.	n.a.	n.a.	n.a.	n.a.	n.a.	n.a.	363.7	399.3

crystallization or melting, which is in line with the limited tendency of this polymer to crystallize, as reported in the literature [53].

The T_gs measured on the neat polymers are similar to those found in the PLA/PPeF blends. PLA's T_g in the blends is located between 58.7 °C and 54.4 °C, with a slight decrease with increasing PPeF content. The same is observed on cooling and in the second heating scan (not reported for brevity). PPeF's T_g in the blends, detectable only for high PPeF concentrations, is located at approx. 14 °C. This confirms the persistent immiscibility of the blends, in good agreement with SEM observations, even though the slight decrease in PLA's T_g suggests a partial compatibilization. However, it is very difficult to estimate the miscibility and the compatibilization degrees from such small shifts [54]. The crystallinity of the as-produced neat PLA sheets is approx. 21.4 %, and it halves (12.1 %) when 1 phr Joncryl is added. On the other hand, PPeF does not affect the crystallizability of PLA in the first heating scan. These DSC results are in good agreement with previous works on PLA/PAF blends compatibilized with Joncryl [33,34].

The thermal stability of the samples has been evaluated between 30 °C and 700 °C through TGA tests performed in a controlled nitrogen atmosphere, and the main results are reported in Fig. 4b and Table 3. None of the samples present any significant

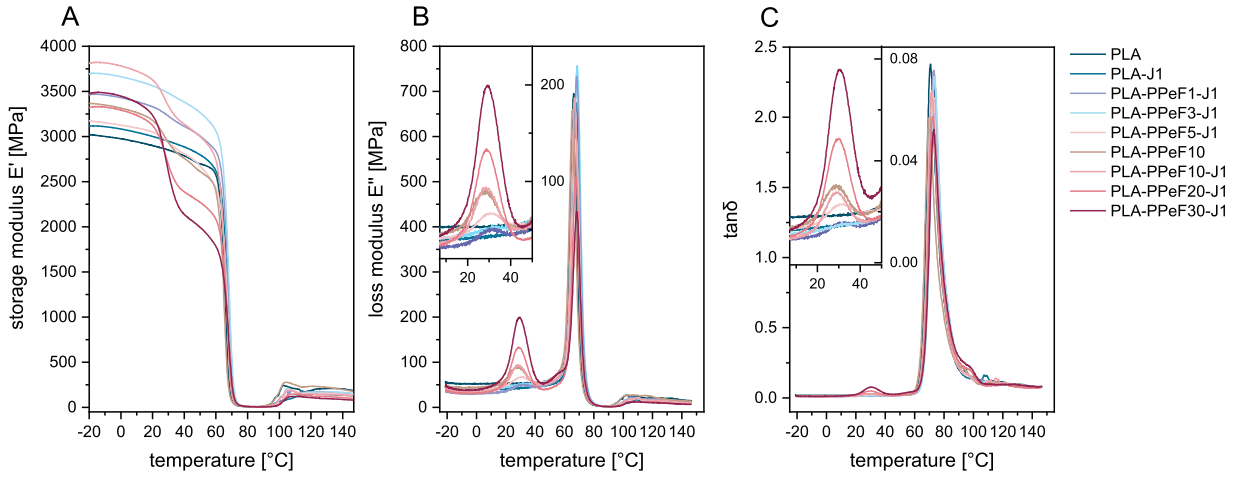

Fig. 5

DMTA thermograms of the prepared blends. Trends of (a) storage modulus; (b) loss modulus; (c) *tanδ* as a function of temperature.

mass loss at around 100 °C, therefore indicating the absence of adsorbed water and, thus, effective storage in dry conditions. PLA is characterized by a T_d of 378.8 °C, while PPeF degrades at a higher temperature, i.e., 399.3 °C. The introduction of Joncryl in PLA (PLA-J1) causes a slight decrease in T_d, which is probably caused by a decrease in crystallinity.

Even though PPeF is more thermally stable than PLA, an increase in the PPeF content causes a decrease in T_{onset} and T_d. For example, T_d reaches value of 361.5 °C for PLA-PPeF30-J1 (−17 °C than neat PLA). Moreover, slower degradation rates are observed. Nevertheless, the degradation of all samples occurs in a narrow temperature range comprised between 360 °C and 400 °C, which is significantly higher than the process temperatures employed in this work and the service temperatures required in packaging applications. Interestingly, the DTG curve of PLA-PPeF30-J1 shows the presence of a first main peak at the degradation of the PLA-rich phase, followed by a shoulder in correspondence of the T_d of PPeF, which is once again representative of the blend immiscibility.

The dynamic mechanical analysis allowed the determination of the storage modulus (E'), the loss modulus (E'') and the loss factor ($tan\delta$) as a function of temperature for all the prepared samples (Fig. 5(a–c)). Neat PLA is characterized by an E' close to 3 GPa at low temperature, which abruptly decreases at the glass transition region (approx. 60 °C), to reach values of approx. 7.0 MPa at 80 °C. This decrease is preceded by a small hump, associated to an enthalpic relaxation of the polymer chains [55]. In the rubbery plateau, PLA chains have sufficient mobility to reorganize in crystalline domains, which leads to cold crystallization associated to an increase in E', in good agreement with DSC results. The introduction of 1 phr Joncryl (PLA-J1) leads to an increase in E' especially at low temperatures - which can be associated to an increase in molecular weight - but has little effect on the rest of the DMTA thermogram.

All the transitions detected in PLA are also visible in all the prepared blends. Notably, the same stiffening effect at low temperatures caused by J is also observable by comparing PLA-PPeF10 and PLA-PPeF10-J1. On the other hand, the role played by PPeF is less clear. For example, the value of E' below the glass transition temperature of both polymers does not show an evident trend with the PPeF concentration. On the other hand, at the PPeF's T_g, E' shows a manifest inflection, which is increasingly evident with an increase in the PPeF concentration. This inflection is accompanied by peaks in the E'' and $tan\delta$ thermograms (Fig. 5(b–c)), which increase with the PPeF concentration. What remains constant is instead the position of these peaks. As reported in Table 4, the location of the two E'' peaks, identified with the T_gs of the PLA and PPeF phase, do not remarkably vary with the blend composition, thus highlighting, once again, the blend immiscibility.

Table 4

Results of the DMTA tests on the prepared blends form the E'' peaks.

Sample	T_g^{PPeF}	T_g^{PLA}
PLA	n.a.	66.3
PLA-J1	n.a.	67.9
PLA-PPeF1-J1	31.9	68.4
PLA-PPeF3-J1	32.6	68.7
PLA-PPeF5-J1	31.0	67.9
PLA-PPeF10	28.0	67.9
PLA-PPeF10-J1	28.5	66.9
PLA-PPeF20-J1	28.8	67.6
PLA-PPeF30-J1	29.3	68.2

3.4 Mechanical properties

The results of the quasi-static tensile tests are reported in Fig. 6(a–c) and Table 5. Neat PLA shows a typical behavior reported many times in the literature, i.e., an elastic modulus (E) of 3.1 GPa, a mechanical strength of 62.2 MPa, and a sudden, catastrophic failure at a strain of 5.0 %, which denotes a brittle behavior with no signs of yielding.

The situation changes considerably by adding PPeF and Joncryl. The addition of Joncryl to PLA causes a slight increase in ductility, likely due to a decrease in crystallinity. With an increase in PPeF content, the stiffness decreases (down to 1.9 GPa for PLA-

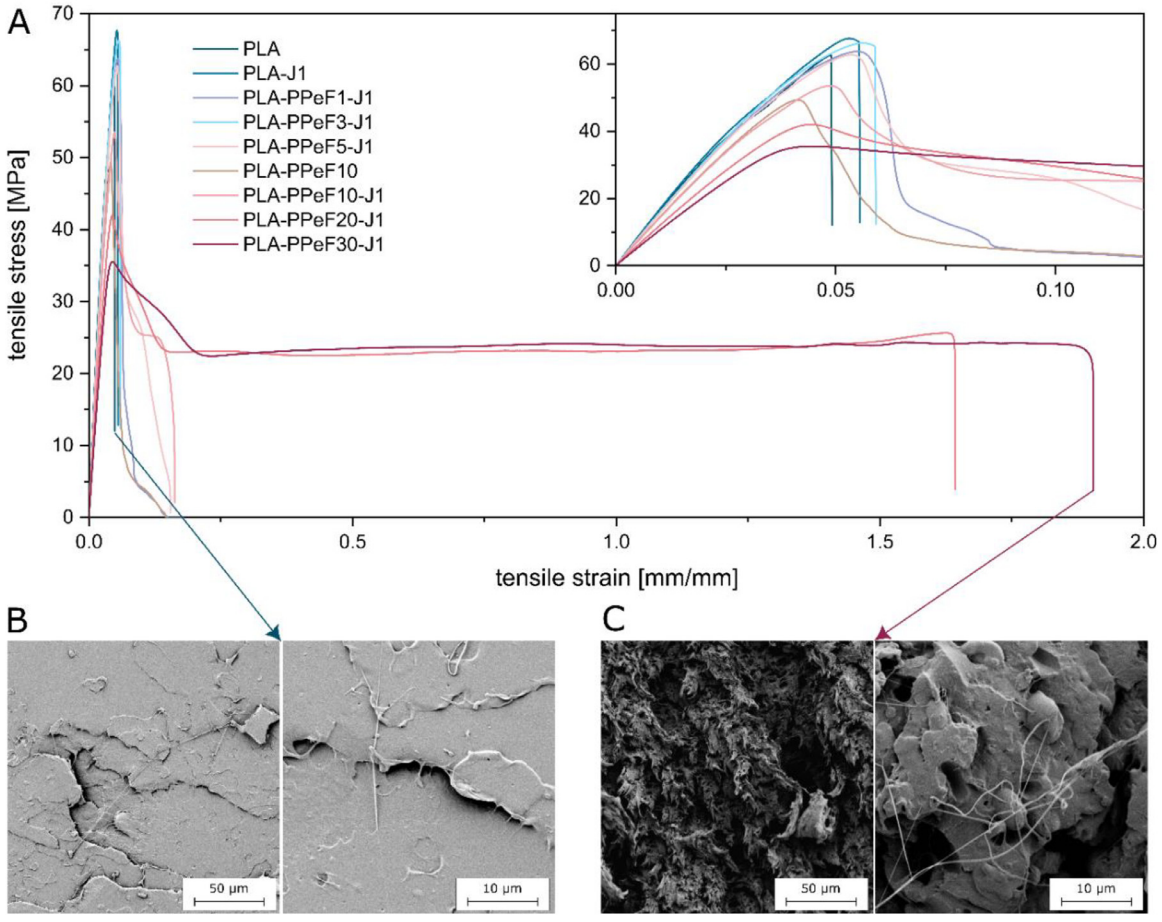

Fig. 6

(a) Representative tensile stress-strain curves obtained in quasi-static tensile tests on the prepared blends; (b) SEM micrographs of the tensile fracture surface of PLA at two magnifications; (c) SEM micrographs of the tensile fracture surface of PLA-PPeF30-J1 at two magnifications.

Table 5

Main results of the quasi-static tensile tests on the prepared blends. n.d. = not detectable.

Sample	E (GPa)	σ_y (MPa)	ε_y (%)	σ_{MAX} (MPa)	$\varepsilon(\sigma_{MAX})$ (%)	σ_b (MPa)	ε_b (%)
PLA	3.1 ± 0.1	n.d.	n.d.	62.2 ± 1.9	4.9 ± 0.2	62.2 ± 1.9	5.0 ± 0.3
PLA-J1	3.3 ± 0.1	n.d.	n.d.	65.5 ± 1.2	5.1 ± 0.2	63.2 ± 1.1	5.5 ± 0.3
PLA-PPeF1-J1	3.1 ± 0.2	n.d.	n.d.	65.3 ± 1.9	5.4 ± 0.2	65.3 ± 1.9	5.4 ± 0.3
PLA-PPeF3-J1	3.3 ± 0.2	n.d.	n.d.	65.7 ± 1.4	5.3 ± 0.2	65.7 ± 1.4	5.7 ± 0.3
PLA-PPeF5-J1	3.1 ± 0.2	61.2 ± 0. 9	5.3 ± 0.1	61.1 ± 1.0	5.3 ± 0.1	32.7 ± 9.2	8.4 ± 1.3
PLA-PPeF10	2.6 ± 0.2	n.d.	n.d.	50.2 ± 0.7	4.3 ± 0.1	50.2 ± 0.7	4.3 ± 0.1
PLA-PPeF10-J1	2.8 ± 0.1	53.0 ± 0.7	4.7 ± 0.1	53.0 ± 0.7	4.7 ± 0.1	24.9 ± 1.0	12.5 ± 1.4
PLA-PPeF20-J1	2.4 ± 0.1	42.7 ± 0.8	4.5 ± 0.1	42.7 ± 0.8	4.5 ± 0.1	25.5 ± 0.9	150 ± 50
PLA-PPeF30-J1	1.9 ± 0.1	35.7 ± 0.6	4.5 ± 0.1	35.7 ± 0.6	4.5 ± 0.1	25.2 ± 1.4	200 ± 70

PPeF30-J1) and the tensile behavior becomes more ductile, with an evident yield point and a progressively increasing strain at break. Remarkably, after an evident plastic plateau given by a necking propagation involving the whole specimen, the values of ε_b reach values of 200 % for PLA-PPeF30-J1, and the tensile fracture surface evidences the signs of plasticization, not present in neat PLA (Fig. 6(b,c)). Notably, PPeF can perform this plasticization effect only when the blend is compatibilized, which is evident by comparing the stress-strain curves of PLA-PPeF10 and PLA-PPeF10-J1. This indicates the fundamental role of Joncryl in promoting a finer dispersion of PPeF domains and a stronger interfacial interaction with the surrounding PLA matrix, which both promote the load transfer from PLA to the PPeF phases, allowing effective plasticization. As suggested by other works in the literature on PLA toughening by a second polymer phase, a biphasic, immiscible blend with soft domains finely dispersed in a stiff matrix is here a fundamental condition to promote effective toughening [33,56]. The observed increase in ductility of PLA-

Table 6

Main results of the EWF tests performed on the prepared samples.

Sample	w_e (kJ/m^2)	βw_p (MJ/m^3)	R^2	$w_{e,ini}$ (kJ/m^2)	$w_{e,prop}$ (kJ/m^2)
PLa-PPeF5-J1	6.2 ± 2.7	3.1 ± 0.3	0.91	2.4 ± 1.2	3.8 ± 3.3
PLa-PPeF10	8.3 ± 2.6	2.9 ± 0.3	0.92	3.8 ± 1.6	4.6 ± 2.9
PLa-PPeF10-J1	21.0 ± 2.0	1.9 ± 0.2	0.85	5.3 ± 0.8	15.7 ± 1.8
PLa-PPeF20-J1	32.0 ± 3.8	2.5 ± 0.3	0.87	6.5 ± 1.3	25.5 ± 1.4
PLa-PPeF30-J1	40.0 ± 4.4	2.2 ± 0.7	0.73	7.0 ± 1.3	33.0 ± 4.1

PPeF10-J1 compared to PLA-PPeF10 can also be partially due to a decrease in crystallinity of the PLA phase, although this alone wound not be sufficient to explain such an increase in strain at break, given the modest increase in ε_b of PLA-J1 compared to neat PLA. Overall, these results suggest that PPeF is effective as a toughening agent for PLA and, given its effects on all the mechanical parameters, its concentration must be chosen as a function of the target properties, to reach the desired balance between stiffness, strength, and ductility.

Given the promising results obtained in the tensile tests, the essential work of fracture (EWF) approach was adopted to investigate the mechanical behavior more deeply. The EWF tests allowed evaluating the role of PPeF and Joncryl on the post-yield fracture mechanics of PLA. This is particularly important for biopolymer films intended for packaging applications, as poor resistance to fracture propagation can be detrimental not only from the mechanical point of view but also because it may cause a decrease in the gas barrier performance. Hence, increasing the infamously poor fracture toughness of PLA is key to expanding its range of applications in the flexible packaging field.

The EWF test has been carried out on all the prepared compositions, but the results were assumed valid if σ_{max} for each specimen was comprised between 0.9 and 1.1 times the average value of the tensile yield stress, to ensure that the fracture process occurred only after a complete yielding of the ligament zone [41]. This condition was satisfied only for the samples with a PPeF fraction higher than 5 wt %, while for the other samples the ligament was not fully yielded, showing the propagation of unstable cracks and making the post-yield fracture mechanics theory not applicable, as also reported elsewhere in the literature for PLA [57–59]. Hence, the results of this test were determined only for samples with a PPeF fraction higher than 5 wt %.

Fig. 7(a–e) shows representative load-displacement curves obtained from EWF tests on DENT specimens. For all curves, the load increases with the displacement until a maximum, at which the crack starts propagating until the coverage of the whole ligament length. As expected, the value of specific work of fracture (Fig. 7(f–j)) increases with the ligament length, and from these data it is possible to calculate w_e and βw_p (see Eqs. (2–4)). The values of w_e (Table 6) considerably increase with the PPeF fraction, from 6.2 kJ/m^2 of the sample PLA-PPeF5-J1 up to 40.0 kJ/m^2 of the sample PLA-PPeF30-J1, while the non-essential component (βw_p) does not significantly increase. These values of w_e are higher than those found in the literature for similar PLA grades processed from the melt, equal to approx. 5 kJ/m^2 [57,59], reported as a qualitative comparison even though the authors underlined that the EWF approach was not applicable to PLA. This demonstrates the effectiveness of PPeF as a toughening agent for PLA. Moreover, the role of Joncryl can be appreciated by comparing the values of w_e for PLA-PPeF10, equal to 8.3 kJ/m^2, and that of PLA-PPeF10-J1, equal to 21.0 kJ/m^2, which is in good agreement with the tensile tests results and once again confirms the key role of this compatibilizer in promoting a finer dispersion and higher interfacial adhesion of the flexible second phase [29].

Additionally, the specific essential work of fracture initiation ($w_{e,in}$), reported in Table 6, does not significantly vary with the composition, while the specific essential work of fracture propagation ($w_{e,prop}$) increases with the PPeF amount, up to 33.0 kJ/m^2 for PLA-PPeF30-J1. This implies that much more energy must be spent to propagate the fracture across this blend, probably because the stress concentration promoted by the PPeF domains induces micro-deformations in the matrix, which orient the PLA chains and hinder the production of new surfaces. Overall, these data demonstrate the effectiveness of PPeF in toughening PLA and suppressing crack propagation, helping to produce PLA-based films with comparable or in most cases superior w_e values than those produced with other toughening agents reported in the literature [57,59-62].

3.5 Functional properties

Transmittance tests were carried out as the optical transparency in the visible range can be a very interesting property, especially for packaging applications. Fig. 8a shows the transmittance spectra of the film samples, while Fig. 8b shows the pictures of the films, to visually show the optical transparency. Neat PLA, PLA-J1, and neat PPeF feature high transmittance values thanks to their low degree of crystallinity. On the other hand, the transmittance decreases with an increase in the PPeF concentration, as expected given the immiscible and biphasic nature of the blends.

Remarkably, PPeF shows a very low transmittance in the UV region, especially below 300 nm, due to the UV absorption capacity of furan rings conjugated with carbonyl groups. A strong UV absorption is very positive for packaging applications as the UV light, already at 380 nm, has enough energy to induce autoxidation of fats, degradation of vitamins, and discoloration of fresh meat, thereby lowering the food quality. Therefore, the optimal food packaging material couples strong UV barrier properties with transparency in the visible range. It is interesting to notice that an amount of PPeF as low as 1–3 wt % can impart these UV-barrier properties to the film, while retaining most of the transparency in the visible range. Hence, as already observed for other furanoate polyesters blended with PLA [24,33], PPeF is an

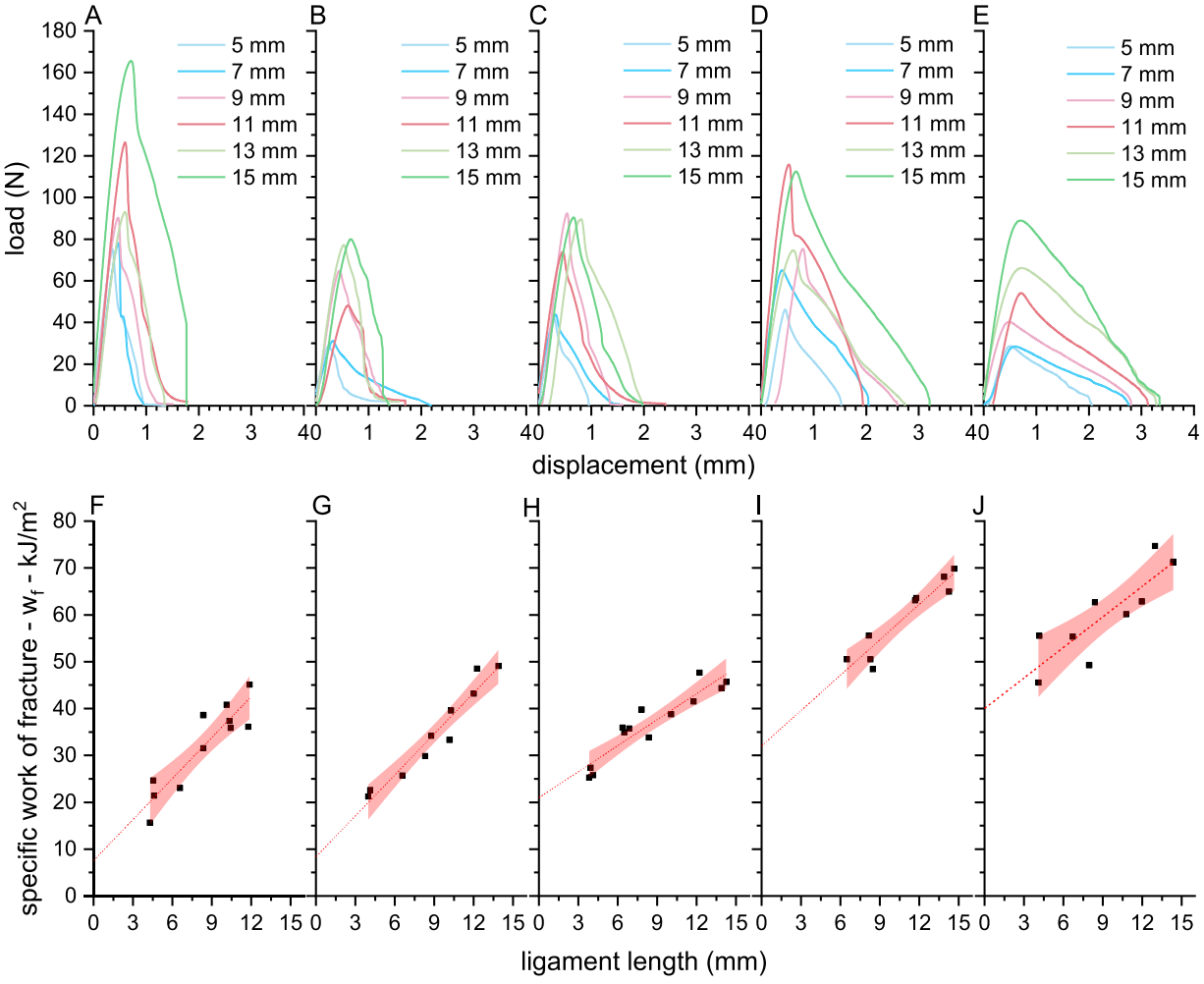

Fig. 7

Results of the EWF tests on the prepared films. Representative load-displacement curves of (a) PLA-PPeF5-J1; (b) PLA-PPeF10; (c) PLA-PPeF10-J1; (d) PLA-PPeF20; (e) PLA-PPeF30-J1. Specific specific work of fracture as a function of the ligament length of (f) PLA-PPeF5-J1; (g) PLA-PPeF10; (h) PLA-PPeF10-J1; (i) PLA-PPeF20; (j) PLA-PPeF30-J1. Dashed lines represent the linear fitting and the shaded zone is the 95 % confidence interval.

active additive useful for the production of packaging films with strong UV-barrier properties.

It is important to point out that, as stated in the Materials and Methods section, the tested films had a thickness variable between 85 μm and 225 μm, which may have affected the exact values of the measured optical transmittance. However, the most important results of the test, i.e., the role played by PPeF in improving the UV shielding properties of PLA, still holds, and so do its practical implications.

Fig. 9 shows the OTR values for the prepared films. Given that the films prepared for this test had thicknesses variable between 85 μm and 225 μm, as the different values of viscosity of the blends prevented the production of films with homogeneous thickness across the compositions, the OTR values were multiplied by the thickness in μm and divided by 100, so to convert the OTR values given by the instrument (the "permeance", measured in cm^3/(m^2·d·bar)) into OTR values for a 100-μm film (the "permeability", measured in (cm^3·100 μm)/(m^2·d·bar)). Although the followed standard (ASTM D1434–23) recommends calculating normalized permeability values only if "the constancy of the permeability has been verified using several different thicknesses of the material", which has not been done in this work, this normalization procedure was the only one available to produce OTR values comparable to one another. Moreover, the described normalization procedure, although not explicitly declared, has been applied elsewhere in the literature on films of similar materials [35,63,64]. The calculated OTR for PLA is in line with that reported elsewhere in the literature [24,34], while the addition of J does not considerably modify the OTR value, although the slight increase in the average value may be ascribed to a decreased crystallinity. The addition of PPeF improves the gas barrier properties of the prepared films thanks to the remarkable gas barrier properties of PPeF [22], with the composition PLA-PPeF30-J1 showing an OTR of 111 (cm^3·100 μm)/(m^2·d·bar), with a reduction of 37 % compared to neat PLA. This is remarkable, considering that the PPeF phase is discontinuous due to the sea island microstructure evident in SEM micrographs (see Fig. 2) and that the testing temperature is above its T_g, where the gas barrier

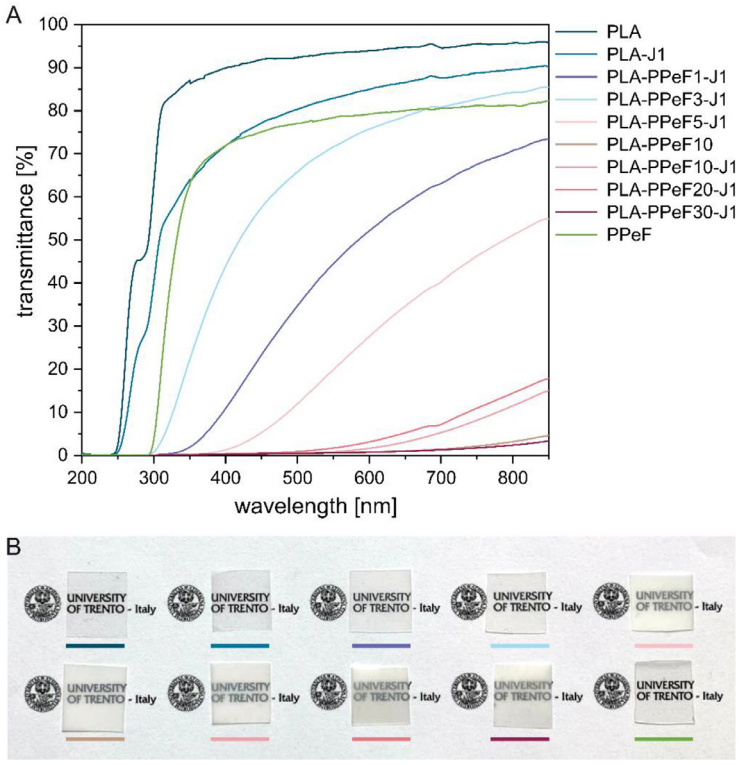

Fig. 8

(a) Optical transmittance of the prepared films as a function of the wavelength of the incident radiation, evaluated through UV–VIS spectrophotometry, (b) pictures of the prepared films to show the optical transparency.

properties of traditional amorphous polymers are notoriously scarce. Conversely, for polymers containing mesogenic groups, such as furanoate polyesters, the absence of crystallinity results in better barrier properties, and this effect is even more pronounced when the glass transition temperature is around room temperature, as in the case here presented. This occurs because of the lower interphase content between amorphous and crystalline phases, which allows for the maximization of interchain interactions (primarily pi-pi interactions and pseudo-hydrogen bonding) due to chain mobility at room temperature [22]. To further improve the gas permeation properties of these films, it would be beneficial to further increase the PPeF concentration and/or to promote a co-continuous microstructure across the two polymer phases.

3.6 Evaluation of the degradability in compost

Finally, compost burial tests were carried out to investigate the degradability of the prepared blends. Biodegradation can be schematized in a three-step process. Initially, outside the microbial cell, macromolecular chains are cleaved into oligomers and monomers, then the low molecular weight products migrate inside the microbial cells, and finally they are metabolized, the respiration of biomass consuming O_2 and producing CO_2 and H_2O (under aerobic conditions). Almost all standardized methods for determining biodegradation (e.g., ISO 19,679:2020, ISO 17,556:2019, ISO 14,855–2:2018, ISO 14,855–1:2005) are focused on the measurement of the conversion into CO_2 of the organic carbon initially present in the plastic. On the other hand, in the literature, most of the papers concerning biodegradation of polymers, blends or composites are based on weight loss monitoring that is accepted as a biodegradability index of plastic films [65]. Whenever WL is used to monitor the degradation of polymer samples, just the first step of the biodegradation process is involved, i.e., macromolecular chain depolymerization into oligomers that are eroded from the surface.

Compost burial degradation tests were carried out by sandwiching the polymer films between two layers of a mixture of milled perlite and compost, monitoring the WL for up to 60 days. Perlite was used to increase the amount of water retained and accelerate degradation in compost. Fig. 10a shows the average weight loss vs. the compost burial degradation time of neat PLA and of some selected blends. Surprisingly, PPeF is the most susceptible to microorganisms in compost, reaching a WL of 26.4 ± 1.5 % in 60 days with a linear increment as a function of time, significant reductions in film thickness and appearance of well-visible holes. This confirms the degradability of PPeF in composting conditions, as described in our previous work [64], which opens new and exciting perspectives for the widespread application of this biopolymer in combination with rigid compostable biopolymers.

Up to 45 days of compost burial test, the WL of the PLA-J1 specimens and of the selected blends are almost equal to zero. Reasonably, the initial hydrolytic process, highlighted by the variations in SCA values (Fig. 10b), has not yet generated chain segments short enough to be eroded from the surface. In fact, no variations in thickness can be observed. After 60 days of the

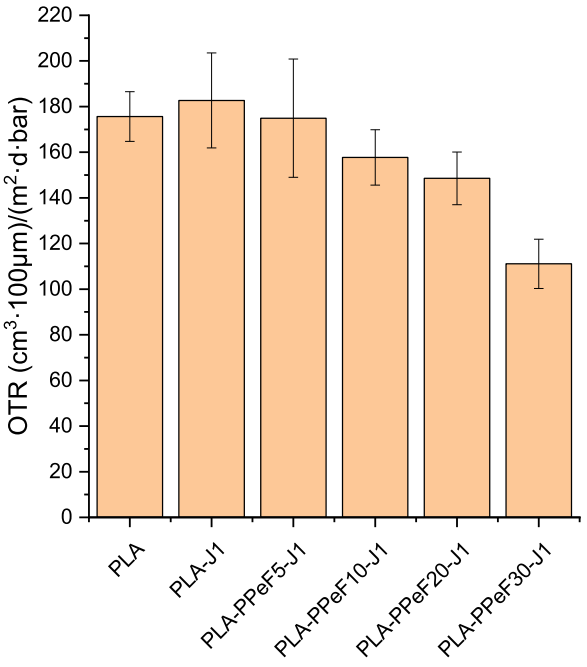

Fig. 9

Oxygen permeation properties of some selected compositions. OTR values at 25 °C.

induction period, an appreciable increase is recorded for PLA-J1 and a small one for its blends. However, SCA measurements highlight a relevant increase in wettability reasonably related to the formation of hydrolytic chain ends. Chemical modifications on the surface of the thin films, induced by degradation in compost, increase plastic samples wettability, highlighted by CA decrease (Fig. 10b) and, consequently, the microbial susceptibility is encouraged with a lower degradation rate for the blends. The presence of chain branching and extension, put in evidence by the rheological characterization, could partially justify the low degradation rate in compost.

4 Conclusions

This work demonstrates the effective toughening and compatibilization of PLA/PPeF blends for the development of novel eco-sustainable packaging films with enhnaced physical properties. The addition of 1 phr Joncryl compatibilizer promoted finer dispersion of PPeF domains and improved interfacial adhesion in the blends. Incorporating up to 30 wt % PPeF induced remarkable ductility enhancements, increasing strain at break from 5 % for neat PLA up to 200 % for PLA-PPeF30-J1. Quasi-static tensile tests proved the key role of Joncryl in enabling effective property improvements.

Through the essential work of fracture (EWF) approach, the specific essential work of fracture (w_e) was found to rise from 6.2 to 40.0 kJ/m^2 with increasing PPeF content, confirming its potency as a toughness enhancer. This also mostly derived from the essential work of fracture propagation term (w_{prop}), indicating PPeF suppression of crack growth. Oxygen permeability declined by 37 % for PLA-PPeF30-J1 compared to neat PLA owing to the outstanding barrier properties of PPeF. Adding just 1–3 wt % PPeF also imparted strong UV-barrier capability.

Moreover, PPeF exhibited 26 % weight loss after 60 days in compost burial tests, proving its degradability. Hence, PLA/PPeF blends offer an optimal balance of stiffness, ductility, fracture toughness, barrier performance, and sustainability. Further property enhancements may be achievable through finer phase control and morphology tailoring. Nonetheless, these high-

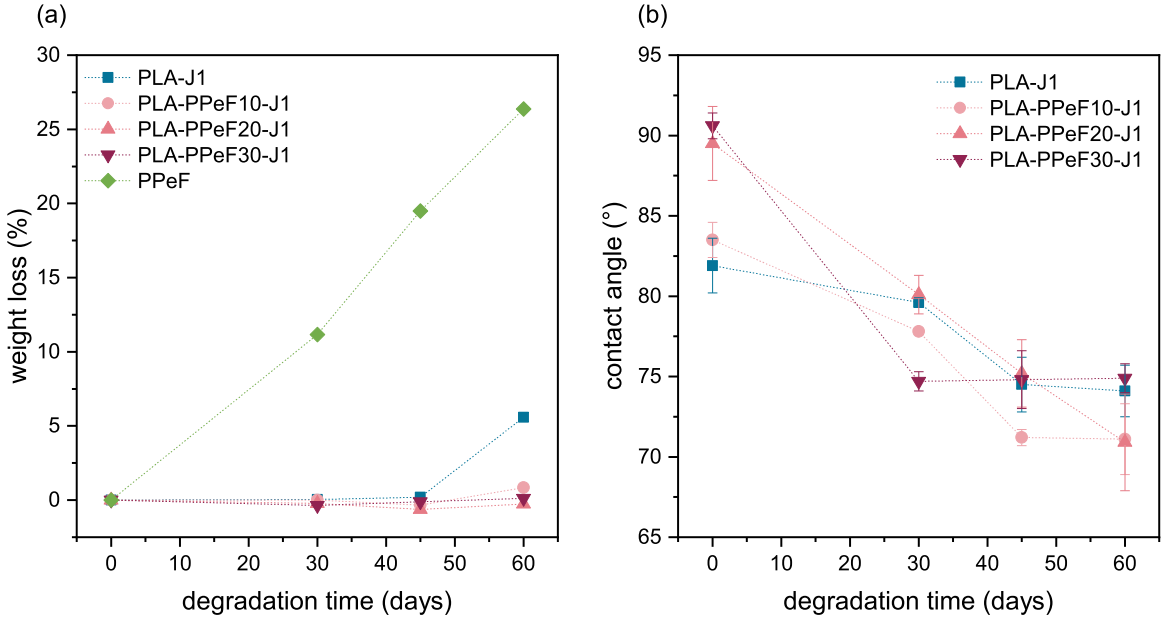

Fig. 10

Results of the compost burial test at 58 °C for some selected samples. (a) Average weight loss percentage vs. degradation time; (b) static contact angle values vs. degradation time.

performing blends display promise for flexible food packaging applications to help advance sustainability.

Declaration of competing interest

The authors declare that they have no known competing financial interests or personal relationships that could have appeared to influence the work reported in this paper.

Data availability

Data will be made available on request.

CRediT authorship contribution statement

Giulia Fredi: Writing – review & editing, Writing – original draft, Visualization, Methodology, Investigation, Funding acquisition, Formal analysis, Data curation, Conceptualization. **Davide Perin:** Writing – review & editing, Visualization, Validation, Methodology, Investigation, Data curation. **Carlotta Zardo:** Investigation. **Marco Rapisarda:** Writing – review & editing, Investigation, Formal analysis. **Paola Rizzarelli:** Writing – review & editing, Methodology, Investigation, Formal analysis. **Michelina Soccio:** Writing – review & editing, Methodology, Investigation, Funding acquisition, Data curation. **Nadia Lotti:** Writing – review & editing, Supervision, Methodology, Funding acquisition. **Andrea Dorigato:** Writing – review & editing, Supervision, Resources, Funding acquisition.

Acknowledgements

Biofactory S.p.A (Calcinate, BG, Italy) is gratefully acknowledged for providing the compost for soil burial tests. This research activity has been funded by Fondazione Cassa di Risparmio di Trento e Rovereto (CARITRO, grant number 2020.0265). M.S., and N.L. acknowledge the Italian Ministry of University and Research. This publication is based upon work from COST Action FUR4Sustain, CA18220, supported by COST (European Cooperation in Science and Technology).

References

[1] K.J. Groh, T. Backhaus, B. Carney-Almroth, B. Geueke, P.A. Inostroza, A. Lennquist, et al., Overview of known plastic packaging-associated chemicals and their hazards, Sci. Total Environ. 651 (2019) 3253–3268.

[2] S. Devasahayam, G. Bhaskar Raju, C. Mustansar Hussain, Utilization and recycling of end of life plastics for sustainable and clean industrial processes including the iron and steel industry, Mater. Sci. Energy Technol. 2 (2019) 634–646.

[3] A. Meraldo, 4 - Introduction to bio-based polymers, in: JR Wagner (Ed.), Multilayer Flexible Packaging, 2nd Edition, William Andrew Publishing, 2016, pp. 47–52.

[4] E. White, R. Bassilakis, S. Nogués, From the Plastics Present to a Sustainable future: The bioplastics Innovation landscape, Players and Market Opportunities, Clarivate™, 2020.

[5] M. Konstantopoulou, Z. Terzopoulou, M. Nerantzaki, J. Tsagkalias, D.S. Achilias, D.N. Bikiaris, et al., Poly(ethylene furanoate- co -ethylene terephthalate) biobased copolymers: synthesis, thermal properties and cocrystallization behavior, Eur. Polym. J. 89 (2017) 349–366.

[6] M. Niaounakis, Biopolymers Reuse, Recycling, and Disposal, William Andrew Publishing, 2013.

[7] G. Fredi, A. Dorigato, Recycling of bioplastic waste: a review, Adv. Ind. Eng. Polym. Res. 4 (2021) 159–177.

[8] Z. Liu, Y. Wang, B. Wu, C. Cui, Y. Guo, C. Yan, A critical review of fused deposition modeling 3D printing technology in manufacturing polylactic acid parts, Int. J. Adv. Manuf. Technol. 102 (2019) 2877–2889.

[9] A. Pegoretti, L. Fambri, C. Migliaresi, In vitro degradation of poly(L-lactic acid) fibers produced by melt spinning, J. Appl. Polym. Sci. 64 (1997) 213–223.

[10] M. Tait, A. Pegoretti, A. Dorigato, K. Kaladzidou, The effect of filler type and content and the manufacturing process on the performance of multifunctional carbon/poly-lactide composites, Carbon N Y 49 (2011) 4280–4290.

[11] E. Balla, V. Daniilidis, G. Karlioti, T. Kalamas, M. Stefanidou, N.D. Bikiaris, et al., Poly(lactic Acid): a versatile biobased polymer for the future with multifunctional properties-from monomer synthesis, polymerization techniques and molecular weight increase to PLA applications, Polymers (Basel) 13 (2021).

[12] G. Perego, G.D. Cella, C. Bastioli, Effect of molecular weight and crystallinity on poly(lactic acid) mechanical properties, J. Appl. Polym. Sci. 59 (1996) 37–43.

[13] H. Xu, J. Zhou, K. Odelius, Z. Guo, X. Guan, M. Hakkarainen, Nanostructured phase morphology of a biobased copolymer for tough and UV-resistant polylactide, ACS Appl. Polym. Mater. 3 (2021) 1973–1982.

[14] J.J. Bozell, G.R. Petersen, Technology development for the production of biobased products from biorefinery carbohydrates—the US department of energy's "Top 10" revisited, Green Chem. 12 (2010) 539.

[15] S. Paszkiewicz, K. Walkowiak, I. Irska, S. Mechowska, K. Stankiewicz, A. Zubkiewicz, et al., Influence of the multiple injection moulding and composting time on the properties of selected packaging and furan-based polyesters, J. Polym. Environ. 31 (2022) 722–742.

[16] X. Fei, J. Wang, X. Zhang, Z. Jia, Y. Jiang, X. Liu, Recent Progress on Bio-Based Polyesters Derived from 2,5-Furandicarbonxylic Acid (FDCA), Polymers (Basel) 14 (2022) 625.

[17] H.T.H. Nguyen, P. Qi, M. Rostagno, A. Feteha, S.A. Miller, The quest for high glass transition temperature bioplastics, J. Mater. Chem. A 6 (2018) 9298–9331.

[18] L. Shang, S. Qu, Y. Deng, Y. Gao, G. Yue, S. He, et al., Simple furan-based polymers with the self-healing function enable efficient eco-friendly organic solar cells with high stability, J. Mater. Chem. C 10 (2022) 506–516.

[19] G. Fredi, A. Dorigato, Compatibilization of biopolymer blends: a review, Advanced Industrial and Engineering Polymer Research, 2023 In press.

[20] Z. Terzopoulou, A. Zamboulis, L. Papadopoulos, M.E. Grigora, K. Tsongas, D. Tzetzis, et al., Blending PLA with polyesters based on 2,5-furan dicarboxylic acid: evaluation of physicochemical and nanomechanical properties, Polymers (Basel) 14 (2022) 4725.

[21] T.P. Dos Santos, K.B. Dias, E. Bischoff, R.S Mauler, Synthesis of esters derived from 2,5-furandicarboxylic acid and study of its plasticizing effects on poly(lactic acid), J. Polym. Res. 29 (2022) 58.

[22] G. Guidotti, M. Soccio, M.-C. García-Gutiérrez, E. Gutiérrez-Fernández, T.A. Ezquerra, V. Siracusa, et al., Evidence of a 2D-ordered structure in biobased poly(pentamethylene furanoate) responsible for its outstanding barrier and mechanical properties, ACS Sustain. Chem. Eng. 7 (2019) 17863–17871.

[23] A.F. Sousa, A.J.D. Silvestre, Plastics from renewable sources as green and sustainable alternatives, Curr. Opin. Green Sustain. Chem. 33 (2022) 100557.

[24] D. Rigotti, M. Soccio, A. Dorigato, M. Gazzano, V. Siracusa, G. Fredi, et al., Novel biobased polylactic acid/poly(pentamethylene 2,5-furanoate) blends for sustainable food packaging, ACS Sustain. Chem. Eng. 9 (2021) 13742–13750.

[25] C. Siracusa, F. Quartinello, M. Soccio, M. Manfroni, N. Lotti, A. Dorigato, et al., On the selective enzymatic recycling of poly(pentamethylene 2,5-furanoate)/poly(lactic acid) blends and multiblock copolymers, ACS Sustain. Chem. Eng. 11 (2023) 9751–9760.

[26] G. Fredi, A. Dorigato, M. Bortolotti, A. Pegoretti, D.N. Bikiaris, Mechanical and functional properties of novel biobased poly(decylene-2,5-furanoate)/carbon nanotubes nanocomposite films, Polymers (Basel) 12 (2020) 2459.

[27] G. Fredi, M.K. Jafari, A. Dorigato, D.N. Bikiaris, A. Pegoretti, Improving the thermomechanical properties of poly(lactic acid) via reduced graphene oxide and bioderived poly(decamethylene 2,5-furandicarboxylate), Materials (Basel) 15 (2022) 1316.

[28] G. Fredi, M.K. Jafari, A. Dorigato, D.N. Bikiaris, R. Checchetto, M. Favaro, et al., Multifunctionality of reduced graphene oxide in bioderived polylactide/poly(dodecylene furanoate) nanocomposite films, Molecules 26 (2021) 2398.

[29] G. Fredi, D. Rigotti, D.N. Bikiaris, A. Dorigato, Tuning thermo-mechanical properties of poly(lactic acid) films through blending with bioderived poly(alkylene furanoate)s with different alkyl chain length for sustainable packaging, Polymer (Guildf) 218 (2021) 123527.

[30] D. Perin, D. Rigotti, G. Fredi, G.Z. Papageorgiou, D.N. Bikiaris, A. Dorigato, Innovative bio-based poly(lactic acid)/poly(alkylene furanoate) fiber blends for sustainable textile applications, J. Polym. Environ. 29 (2021) 3948–3963.

[31] D. Perin, G. Fredi, D. Rigotti, N. Lotti, A. Dorigato, Sustainable textile fibers made of bioderived polylactide/poly(pentamethylene 2,5-furanoate) blends, J. Appl. Polym. Sci. 139 (2022) 51740.

[32] D. Rigotti, G. Fredi, D. Perin, D.N. Bikiaris, A. Pegoretti, A. Dorigato, Statistical modeling and optimization of the drawing process of bioderived polylactide/poly(dodecylene furanoate) wet-spun fibers, Polymers (Basel) 14 (2022) 396.

[33] G. Fredi, E. Zonta, A. Dussin, D.N. Bikiaris, G.Z. Papageorgiou, L. Fambri, et al., Toughening effect of 2,5-furandicaboxylate polyesters on polylactide-based renewable fibers, Molecules 28 (2023) 4811.

[34] G. Fredi, A. Dorigato, A. Dussin, E. Xanthopoulou, D.N. Bikiaris, L. Botta, et al., Compatibilization of polylactide/poly(ethylene furanoate) (PLA/PEF) blends for sustainable and bioderived packaging, Molecules 27 (2022) 6371.

[35] G. Guidotti, M. Soccio, N. Lotti, V. Siracusa, M. Gazzano, A. Munari, New multi-block copolyester of 2,5-furandicarboxylic acid containing PEG-like sequences to form flexible and degradable films for sustainable packaging, Polym. Degrad. Stab. 169 (2019) 108963.

[36] S. Quattrosoldi, G. Guidotti, M. Soccio, V. Siracusa, N. Lotti, Bio-based and one-day compostable poly(diethylene 2,5-furanoate) for sustainable flexible food packaging: effect of ether-oxygen atom insertion on the final properties, Chemosphere 291 (2022) 132996.

[37] A.B. Martinez, J. Gamez-Perez, M. Sanchez-Soto, J.I. Velasco, O.O. Santana, M. Ll Maspoch, The essential work of fracture (EWF) method – analyzing the post-yielding fracture mechanics of polymers, Eng. Fail. Anal. 16 (2009) 2604–2617.

[38] L.H. Sperling, Introduction to Physical Polymer Science, Wiley, Hoboken, New Jersey, US, 2006.

[39] D. Garlotta, A literature review of poly(lactic acid), J. Polym. Environ. 9 (2001) 63–84.

[40] T. Bárány, T. Czigány, J. Karger-Kocsis, Application of the essential work of fracture (EWF) concept for polymers, related blends and composites: a review, Prog. Polym. Sci. 35 (2010) 1257–1287.

[41] J.G. Williams, M. Rink, The standardisation of the EWF test, Eng. Fract. Mech. 74 (2007) 1009–1017.

[42] K. Prashantha, H. Schmitt, M.F. Lacrampe, P. Krawczak, Mechanical behaviour and essential work of fracture of halloysite nanotubes filled polyamide 6 nanocomposites, Compos. Sci. Technol. 71 (2011) 1859–1866.

[43] A. Dorigato, A. Pegoretti, Fracture behaviour of linear low density polyethylene – fumed silica nanocomposites, Eng. Fract. Mech. 79 (2012) 213–224.

[44] J.S.S. Wong, D. Ferrer-Balas, R.K.Y. Li, Y.-W. Mai, M.L. Maspoch, H.-J. Sue, On tearing of ductile polymer films using the essential work of fracture (EWF) method, Acta Mater. 51 (2003) 4929–4938.

[45] A. Dorigato, D. Perin, A. Pegoretti, Effect of the temperature and of the drawing conditions on the fracture behaviour of thermoplastic starch films for packaging applications, J. Polym. Environ. 28 (2020) 3244–3255.

[46] P. Rizzarelli, C. Puglisi, G. Montaudo, Soil burial and enzymatic degradation in solution of aliphatic co-polyesters, Polym. Degrad. Stab. 85 (2004) 855–863.

[47] M. Rapisarda, M.C. Mistretta, M. Scopelliti, M. Leanza, F.P. La Mantia, P Rizzarelli, Influence of calcium carbonate nanoparticles on the soil burial degradation of polybutyleneadipate-Co-butylenetherephthalate films, Nanomaterials (Basel) 12 (2022) 2275.

[48] Fredi G., Karimi Jafari M., Dorigato A., Bikiaris D.N., Checchetto R., Favaro M., et al. Multifunctionality of reduced graphene oxide in bioderived polylactide/poly(dodecylene furanoate) nanocomposite films. 2021;26:2938.

[49] C. Migliaresi, A. De Lollis, L. Fambri, D. Cohn, The effect of thermal history on the crystallinity of different molecular weight PLLA biodegradable polymers, Clin. Mater. 8 (1991) 111–118.

[50] H. Xie LW, B.G. Li, P. Dubois. Poly(ethylene 2,5-furandicarboxylatembpoly(tetramethylene glycol)) multiblock copolymers: from high tough thermoplastics to elastomers. 2018;155:89–98.

[51] G. Socrates, Infrared and Raman Characteristic Group Frequencies: Tables and Charts, 3rd Edition, 2004.

[52] K. Van de Velde, P. Kiekens, Biopolymers: overview of several properties and consequences on their applications, Polym. Test. 21 (2002) 433–442.

[53] G. Guidotti, Soccio Michelina, García-Gutiérrez Mari-Cruz, Gutiérrez-Fernández Edgar, A. Ezquerra Tiberio, Siracusa Valentina, Munari Andrea, Lotti Nadia, Fully biobased superpolymers of 2,5-furandicarboxylic acid with different functional properties: from rigid to flexible, high performant packaging materials, ACS Sustain. Chem. Eng. 8 (2020) 9558–9568.

[54] B. Imre, B. Pukánszky, Compatibilization in bio-based and biodegradable polymer blends, Eur. Polym. J. 49 (2013) 1215–1233.

[55] Cristea M., Ionita D., Iftime M.M. Dynamic mechanical analysis investigations of PLA-based renewable materials: how are they useful? 2020;13:5302.

[56] Y. Long, R.Y. Zhang, J.C. Huang, J.G. Wang, Y.H. Jiang, G.H. Hu, et al., Tensile property balanced and gas barrier improved poly(lactic acid) by blending with biobased poly(butylene 2,5-furan dicarboxylate), ACS Sustain. Chem. Eng. 5 (2017) 9244–9253.

[57] M. Souri Rudabadi, F. Ashenai Ghasemi, M. Fasihi, P Rajaee, An experimental study on the microstructural, tensile, and fracture properties of biodegradable polylactic acid blended with thermoplastic corn starch filled with halloysite nanotubes, Ind. Crops Prod. 201 (2023).

[58] L. Gao, A.D. Drozdov, The Use of various measurement methods for estimating the fracture energy of PLA (polylactic acid), Materials (Basel) 15 (2022) 8623.

[59] M.M. Mazidi, R. Berahman, A. Edalat, Phase morphology, fracture toughness and failure mechanisms in super-toughened PLA/PB-g-SAN/PMMA ternary blends: a quantitative analysis of crack resistance, Polym. Test. 67 (2018) 380–391.

[60] E.A. Franco-Urquiza, J. Cailloux, O. Santana, M.L. Maspoch, J.C. Velazquez infante, The Influence of the clay particles on the mechanical properties and fracture behavior of PLA/o-MMT composite films, Adv. Polym. Tech. 34 (2014) 21470.

[61] C. Rodríguez, D. Arencón, J. Belzunce, M.L. Maspoch, Small punch test on the analysis of fracture behaviour of PLA-nanocomposite films, Polym. Test. 33 (2014) 21–29.

[62] O.H. Arroyo, M.A. Huneault, B.D. Favis, M.N. Bureau, Processing and properties of PLA/thermoplastic starch/montmorillonite nanocomposites, Polym. Compos. 31 (2010) 114–127.

[63] V. Siracusa, S. Karpova, A. Olkhov, A. Zhulkina, R. Kosenko, A. Iordanskii, Gas transport phenomena and polymer dynamics in PHB/PLA blend films as potential packaging materials, Polymers (Basel) 12 (2020) 647.

[64] E. Bianchi, G. Guidotti, M. Soccio, V. Siracusa, M. Gazzano, E. Salatelli, et al., Biobased and compostable multiblock copolymer of poly(l-lactic acid) containing 2,5-furandicarboxylic acid for sustainable food packaging: the role of parent homopolymers in the composting kinetics and mechanism, Biomacromolecules 24 (2023) 2356–2368.

[65] P. Rizzarelli, F. Degli Innocenti, G. Valenti, M Rapisarda, Biodegradation of green polymer composites: laboratory procedures and standard test methods, in: EA Al-Ahmed, Inamuddin (Eds.), Advanced Applications of Bio-degradable Green Composites, Materials Research Forum LLC, 2020, pp. 1–44.